Identifying the Location of a Single Protein along the DNA Strand Using Solid-State Nanopores

Jae-Seok Yu,[†,§] Min-Cheol Lim,[‡,§] Duyen Thi Ngoc Huynh,[‡] Hyung-Jun Kim,[†] Hyun-Mi Kim,[†] Young-Rok Kim,[*,‡] and Ki-Bum Kim[*,†]

[†]Department of Materials Science and Engineering, Seoul National University, Seoul 151-742, Korea and [‡]Graduate School of Biotechnology and Department of Food Science and Biotechnology, Kyung Hee University, Yongin 446-701, Korea. [§]J.Y. and M.L. contributed equally to this work.

ABSTRACT Solid-state nanopore has been widely studied as an effective tool to detect and analyze small biomolecules, such as DNA, RNA, and proteins, at a single molecule level. In this study, we demonstrate a rapid identification of the location of zinc finger protein (ZFP), which is bound to a specific locus along the length of a double-stranded DNA (dsDNA) to a single protein resolution using a low noise solid-state nanopore. When ZFP labeled DNAs were driven through a nanopore by an externally applied electric field, characteristic ionic current signals arising from the passage of the DNA/ZFP complex and bare DNA were detected, which enabled us to identify the locations of ZFP binding site. We examined two DNAs with ZFP binding sites at different positions and found that the location of the additional current drop derived from the DNA/ZFP complex is well-matched with a theoretical one along the length of the DNA molecule. These results suggest that the protein binding site on DNA can be mapped or that genetic information can be read at a single molecule level using solid-state nanopores.

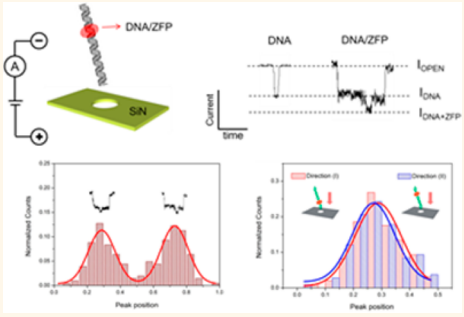

KEYWORDS: nanopore · zinc finger protein · DNA · single molecule · DNA binding protein

Zinc finger proteins (ZFPs) are one of the transcriptional activators and the most common DNA binding motif in all metazoans.[1] Each zinc finger is capable of recognizing three adjacent base pairs in the major groove of double-stranded DNA (dsDNA) *via* a single α-helix with high affinity and sequence specificity.[2] Its DNA recognition is mediated through base contacts with specific amino acids located on the recognition helix. ZFPs typically contain several fingers and three-fingered proteins such as Zif268, and Sp1 recognizes a tract of nine base pairs of dsDNA.[3,4] The diversity in ZFP recognition potential has been expanded by the development of designer zinc fingers and characterization of ZFP-binding properties. Recently, engineered ZFPs with binding ability to a specific DNA sequence have gained a great deal of attention for research, diagnostics, gene therapy, and gene editing.[5−8] Because of the sequence-specific binding nature of ZFPs, long-range haplotype mapping of DNA using engineered ZFPs would be possible. However, there are relatively few technologies to characterize binding affinities of ZFPs for their cognate DNA binding sites and to map the binding locations along the length of DNA. Gel-shift assay is the most common technique to determine the affinity of ZFP toward DNA with a recognition site, but it does not give any information about the exact location to where ZFP binds.[9,10] Fluorescent imaging is another way of imaging the bound protein on DNA,[11,12] but diffraction limitations of optical microscopy and labeling requirements hinder the practical application of this method. Although, atomic force microscopy (AFM) is capable of imaging bound molecules on DNA in high resolution,[7,13−15] its uses are inherently restricted in surface environment and require rather complicated sample preparation processes. Here, we found that solid-state nanopore is an ideal method to identify the position of zinc finger proteins and their binding characteristics to a single protein resolution.

Solid-state nanopores, which have nanometer sized pores fabricated in a mechanically stable membrane,[16] have attracted much interest as a useful device in detection

* Address correspondence to kibum@snu.ac.kr, youngkim@khu.ac.kr.

Received for review February 4, 2015 and accepted May 4, 2015.

Published online May 04, 2015
10.1021/acsnano.5b00784

and analysis of nanometer scale biomolecules due to its advantages of high throughput, high sensitivity, and its simplicity of measurements, namely purely electrical label-free detection.[17,18] Therefore, there are great deals of publications regarding nanopore-based analysis of DNA, RNA, protein, and their interactions as well as potential for a next generation sequencing technology.[19−27] In particular, there were several studies about the detection of DNA binding proteins or polymers such as RecA,[28] bis-PNA,[29] γ-PNA,[30] and *Escherichia coli* SSB.[31] Recently, several groups have reported progress toward the detection of a single protein bound to a DNA using glass and silicon nitride nanopore, allowing them to identify the presence of a target protein and quantification of a modified DNA. Carlsen *et al.* used DNA−protein complexes and found a dependency between nanopore event rate and modified DNA concentration.[32,33] Also, by designing DNA carriers and using biotin−streptavidin binding, Bell *et al.* identified whether the target proteins exist in the mixed solution using a glass nanopore.[32,33] Solid-state nanopores modified with ligand such as aptamer could also detect the target protein by monitoring the elongated translocation time due to the interaction between grafted aptamer and passing protein.[34] Biological nanopores like α-Hemolysin and cytolysin A having asymmetric structure with vestibule were also used to study the conformational heterogeneity and binding kinetics of DNA−protein interaction.[35,36] Symmetric protein nanopore, SP1 (stable protein) having 3 nm of pore-diameter, was also shown to have a potential for detecting ssDNA as well as characterizing the 3D structure of peptides and DNAs by eliminating the vector constriction or direction followed by random passage.[37] To the best of our knowledge, this is the first study for discrimination of DNA-ZFP complexes from pristine DNA to a single protein resolution and identifying the location of a ZFP in a DNA strand without any additional signal amplification and fluorescent labeling. Here, we introduce detection of sequence-specific DNA-binding ZFP using solid-state nanopores. ZFPs can be designed to have strong binding affinities for their cognate DNA binding site and to have novel recognition specificities by protein engineering techniques. For instance, the affinities and specificities of engineered ZFP can be enhanced by addition of structured linkers between zinc fingers and dimerization of fused domains.[38,39] In this work, the engineered ZFP Zif268-NRE with a structural linker was used to recognize the specific DNA sequence of a DNA strand and to demonstrate the possibility of identifying the location of recognition sequence using solid-state nanopore.

Low-stress LPCVD silicon nitride membrane of ~100 nm is transferred on highly insulating Pyrex substrate. Thickness of the transferred membrane is reduced to a desirable level (5−20 nm) by dry etching, and the nanopore is formed using highly focused electron beams.[40] The nanopore chip is then assembled into acrylic fluid cells and is hydrated using a buffered KCl solution. When positive bias voltage is applied across the nanopore by Ag/AgCl electrodes, DNA and the DNA/ZFP complex are caught by an electric field and pass through (translocate) the nanopore. Nanopore fabrication steps and its noise characteristics are described in Figures S1 and S2 (Supporting Information).

Schematic concepts of solid-state nanopore-based identification of DNA−protein interactions are described in Figure 1. When a bare DNA translocates a nanopore, it gives rise to a single step current blockade (ΔI_{DNA}), while ZFP-bound DNA generated an additional peak (ΔI_{ZFP}) due to the extra volume of ZFP. In other words, the increased volume caused by ZFP binding on DNA was successfully reflected by a discrete current blockade peak. Furthermore, by analyzing the ratio of DNA translocation times before (t_1) and after (t_2) the ZFP peak, the position of ZFP binding locus in two different DNAs was analyzed. The low noise characteristics of our solid-state nanopore that was fabricated upon highly insulating substrates[41] enabled us to monitor the location of a single protein that spans around approximately 20 bp along the length of DNA (Figure 1d).

RESULTS AND DISCUSSION

To demonstrate the possibility of identifying the location of protein binding site, we prepared a simple and symmetric dsDNA (520-bp) with ZFP binding site at the center (1-to-1) of the DNA strand. The 520-bp DNA and ZFP were put into an ionic solution of 400 mM KCl, and 100 mV bias voltages were applied across a 4 nm diameter silicon nitride nanopore (5 nm thick). Electrical measurements were performed in 400 mM KCl solution because DNA−protein interactions are very sensitive to salt concentration. ZFP binding to DNA is disrupted at high KCl concentrations over 700 mM, as demonstrated in Figure S3. Because KCl concentration is an important parameter for signal-to-noise ratio in electrical measurements, 400 mM KCl was chosen because ZFP dissociation from the DNA binding site starts to occur at 500 mM KCl. From the translocation data, two types of events were observed. In Figure 2a, representative translocation data, two types of events are shown. One type is a single profile current drop with a relatively short translocation time (Type I), and the other is a translocation event with an additional current spike within a relatively long translocation time (Type II). Current traces are acquired from 100 pM DNA, 8 nm diameter pore, and 10 nm thick SiN and event rate in Figure 2c was acquired from these data.

A scatter plot of current drop *versus* dwell time of all DNA (520 bp)/ZFP translocation events is displayed in Figure 2b. The difference between type (I) and type (II)

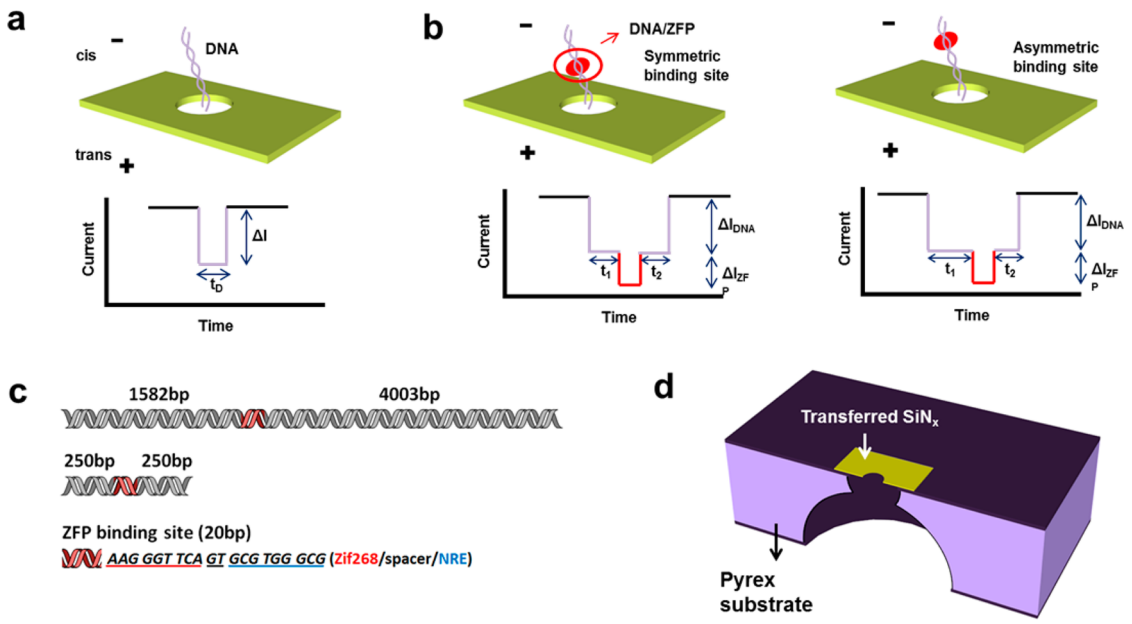

Figure 1. Schematic illustrations of nanopore-based identification of DNA−protein interactions. (a) A translocation event of a bare dsDNA gives rise to a single level current drop. (b) dsDNAs with ZFP binding sites at different parts of the strands display an additional current drop peak in accordance with the binding site. (c) Schematics of two dsDNAs used in this work. One is 5605 bp with a 20 bp binding site at the 2-to-5 position and the other is 520 bp with a 20 bp binding site at the center. (d) Cross-sectional illustration of a low noise solid-state nanopore device used in this work (not to scale).

events is clearly shown. For type (II) events, the maximum magnitude of current drop, namely the gap between the open pore current and the current level of the additional spike ($\Delta I_{DNA} + \Delta I_{ZFP}$) is plotted. The current drop histograms were fitted by a Gaussian function with a mean current drop of ~122 and ~173 pA for type (I) and type (II) events, respectively. The dwell time histogram showed an exponential decay with a mean dwell time of ~136 μs and ~5.86 ms for type (I) and type (II) events, respectively. On the basis of these differences in current drop and dwell time, we assumed that type (I) and type (II) events resulted from bare DNA and DNA/ZFP complex translocations, respectively. It should be noted that although the signal amplitude is not that high due to a low molar concentration (400 mM) and a relatively low applying voltage (100 mV), the signal can be resolved because the rms noise of the present nanopore device is less than 10 pA.

We analyzed the translocation times of type (II) events, which have a characteristic current trace with distinct peaks representing the location of ZFP binding site. The position of ZFP binding site was investigated by assigning the dwell time from the start of the event to the additional current spike as t_1 and from the additional current spike to the end of the event as t_2. A histogram demonstrating the ratio of t_1 and $t_1 + t_2$, which reflects ZFP location on the 520 bp DNA, is presented in Figure 2d. Normalized counts mean the ratio of the number of specific events to total number of events (297 events). From the histogram, one Gaussian distribution with a mean value of 0.513 ± 0.132 was observed. Assuming that the translocation time is proportional to the DNA length, the expected mean $t_1/(t_1 + t_2)$ value is 0.500, which is well matched with the experimental data.

The sequence-specific binding of ZFP on target DNA was also confirmed by AFM.[7] A 520 bp of DNA as used in our nanopore experiment was examined as a template for AFM analysis because short double stranded DNA (approximately 180 nm) with a persistence length of 35 nm[42] is very likely to be present as a linear form, which would facilitate determining the position of bound ZFP on the DNA strand. AFM analysis revealed that the ZFP bound exclusively at the middle of a 520 bp of DNA with a specific binding site spanning from the 251st to the 270th bases (Figure 3b). The height of bound ZFP on the target site is approximately 3 nm whereas that of pristine DNA is approximately 1.6 nm. From these results, it is evident that ZFP binds to the target DNA in sequence-specific manner and the binding site location is represented as the additional current drop within the DNA blockade when analyzed with our solid-state nanopore.

The specific binding properties of ZFP to a target DNA were also confirmed using native polyacrylamide gel electrophoresis. ZFP and DNA harboring specific recognition sequences were incubated at room temperature for 1 h to form DNA/ZFP complexes and then resolved by native polyacrylamide gel electrophoresis. After the gel was stained with EtBr, the DNA location was observed under UV light (Figure 3c,d). As expected, the ZFP binds to the DNA containing its target recognition sequence, and DNA/ZFP complex formation was

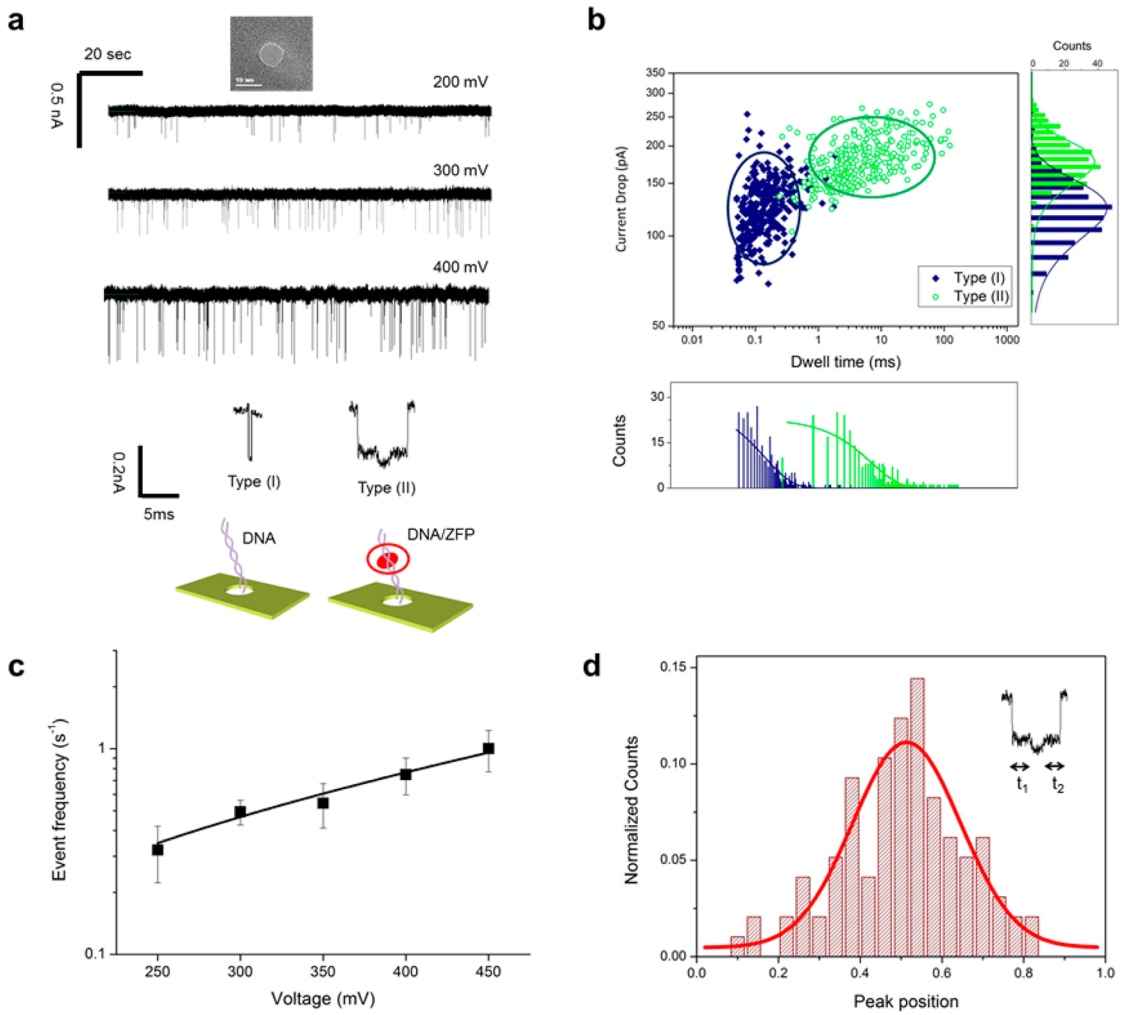

Figure 2. Analysis of DNA (520 bp, binding site at the center) translocation events with ZFP in 400 mM KCl. (a) Current traces from the translocation of DNA-ZFP complex under three different applied voltages. Two types of event signals were detected. Type (I): signals with a single profile current drop. Type (II): signals with an additional current spike. (b) Scatter plot of translocation events for 100 mV applied voltage. Type (I) and type (II) events were indicated as navy diamonds and green circles, respectively. Type (II) events clearly show higher current drop and longer dwell time. (c) The frequency of translocation events as a function of applied voltage, showing an exponential increase in event frequency along with increased applied voltage. (d) Histogram of $t_1/(t_1 + t_2)$, where t_1 is assigned as the dwell time from the start of the event to the additional spike, and t_2 is assigned as the dwell time from the additional spike to the end of the event.

evidenced by decreased mobility. As demonstrated in Figure 3c,d, mobility of the DNA bound with ZFP was lower than that without ZFP. The zinc finger protein location was also examined by staining the gel with coomassie blue (Figure S4b). The band location of ZFP exactly matches that of DNA with a specific binding site in native polyacrylamide gel, implying that the shift was induced by ZFP-DNA complex formation. In other words, DNA/ZFP complex formation decreased DNA mobility at a given bias voltage. The bound ZFP may also partially screen the negative charge of DNA resulting in reduced DNA mobility. The specificity of ZFP to a target DNA was confirmed by reacting the protein with DNA that lacked a recognition sequence. The absence of a gel-shift in the reaction containing ZFP and DNA lacking a recognition sequence implies that the binding reaction is sequence specific. According to the gel electrophoresis and AFM results, it is evident that the type (I) and type (II) events are attributed to the passage of bare DNA and the DNA/ZFP complex, respectively.

Upon confirming the sequence-specific binding between DNA and ZFP, we performed further nanopore experiments to verify the possibility of identifying the specific binding site. We prepared a 5605-bp DNA with a ZFP binding site (20 bp), which was located at the asymmetric position of 2-to-5 (1582 base-to-4003 base) in the DNA strand as shown in Figure 1c. In other words, the length of DNA from one end to the ZFP binding site and from the other end to the ZFP binding site are 1582 bp and 4003 bp, respectively. Figure 4a shows current traces from the translocation of DNA (5605 bp)/ZFP through 8 nm diameter and 10 nm thickness nanopore under three different bias voltages

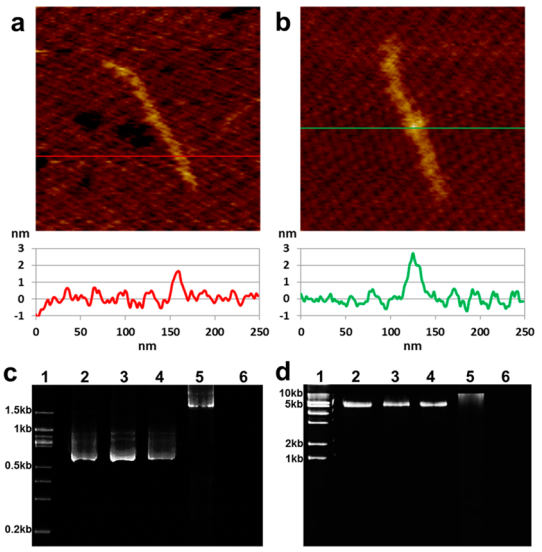

Figure 3. AFM images of bare DNA (a) and the DNA-ZFP complex (b). DNA (520 bp) that was approximately 180 nm in length was used in this analysis. The scan sizes of the images are 250 × 250 nm with Z-scale of 4 nm. Gel-shift assay of 520 bp DNA (c) and 5605 bp DNA (d) in the presence and absence of ZFP. Lane 1, DNA marker; Lane 2, DNA without recognition sequence; Lane 3, DNA without recognition sequence reacted with ZFP; Lane 4, DNA with recognition sequence; Lane 5, DNA with recognition sequence reacted with ZFP; Lane 6, ZFP alone.

and event frequency plot in Figure 4d was acquired from these data.

As was shown earlier in this report, short single level translocation events (type (I)) and long translocation events with an additional current drop (type (II)) were detected. In Figure 4a, representative translocation events of each type are shown. Type (I) events have mean dwell time of 69 μs with $\Delta I/I_O$ = 0.11 (ΔI = magnitude of current drop, I_O = open pore current), which shows similar current drop magnitude and dwell time as those of typical DNA translocation events.[43]

Scatter plot of current drop *versus* dwell time of all translocation events is shown in Figure 4b. The current drop histograms were fitted by a Gaussian function with a mean current drop of ~864 and ~1345 pA for type (I) and type (II) events, respectively. The dwell time histograms showed an exponential decay with a mean dwell time of ~69 μs and ~1.7 ms for type (I) and type (II) events, respectively. The all-point current histogram reveals two distinct peaks, which represent type (I) and type (II) translocation events with a mean amplitude of current blockage of ~831 pA and ~1228 pA, respectively (Figure 4c).

Because a number of researchers have reported quantized level events arising from the translocation of folded DNA,[21,44,45] we conducted further experiments to confirm that the additional current peaks are indeed attributed to ZFP binding, not to folded DNA. Using the same nanopore and ionic solution, we performed translocation experiments with varying voltage conditions (300, 500, and 700 mV). Figure 5b demonstrates the dependency of ΔI_{DNA} and ΔI_{ZFP} on three different applied voltages. Both ΔI_{DNA} and ΔI_{ZFP} linearly increase with applied voltages. We also investigated the ratio between ΔI_{ZFP} and ΔI_{DNA}, which is $\Delta I_{ZFP}/\Delta I_{DNA}$, to confirm that the additional current drop is a reflection of ZFP binding on DNA (Figure 5c). For three different voltage conditions, the value of the $\Delta I_{ZFP}/\Delta I_{DNA}$ is almost constant (~0.355), which implies that the additional current drop came from ZFP binding on DNA. Considering that the translocation of folded DNA typically results in a quantized (2- or 3-fold) current drop,[21,44,45] it is clear that the additional current drop is caused from bound ZFP on the DNA strand.

On the basis of the results that the additional current spike within DNA blockade comes from the ZFP bound on DNA with recognition sequence, it is possible to identify the location of ZFP binding site in tested DNA. As described above, the position of ZFP binding site was investigated by assigning the dwell time from the start of event to the additional spike as t_1 and from the additional spike to the end of event t_2. A histogram demonstrating the ratio of t_1 and $t_1 + t_2$, which reflects the location of the ZFP in DNA, is presented in Figure 6.

As demonstrated in Figure 6a, analysis of the translocations (total 320 events) for DNA with bound ZFP resulted in two Gaussian distributions with a mean value of each $t_1/(t_1 + t_2)$ distribution of 0.287 ± 0.081 and 0.729 ± 0.081. In total, two distinct distributions were probable results because DNA can enter the nanopore in two different directions. When the shorter DNA end enters the nanopore first, we assigned the direction (I), but when the longer DNA end enters first, we assigned the direction (II). As shown in Figure 1c, the DNA used in this study has a ZFP binding site at the 2-to-5 position (1582 base-to-4003 base). In other words, the DNA length from one end to the ZFP binding site and from the other end to the ZFP binding site were 1582 and 4003 bp, respectively. Assuming that the DNA length is proportional to the translocation time, the expected t_1/t_2 values are 0.283 (1582/5585) and 0.717 (4003/5585), which closely correlate with our experimental results (0.287 and 0.729). After normalization, the translocation time ratio was assessed by designating the shorter end of DNA from the ZFP binding site as t_1 and the longer end as t_2. Thus, the mean value of $t_1/(t_1 + t_2)$ for direction (I) and (II) are 0.287 ± 0.082 and 0.271 ± 0.075, respectively (Figure 6b). These results also correlate well with the theoretical value, 0.283.

It is interesting to note that the mean $t_1/(t_1 + t_2)$ value is slightly larger than expected (0.283) in direction (I) (0.287) and smaller in direction (II) (0.271). The same phenomenon was observed in 520-bp DNA with ZFP that is bound at the center of the DNA. The mean value of $t_1/(t_1 + t_2)$ for the DNA with bound ZFP in a symmetric position was 0.513 ± 0.132. These results

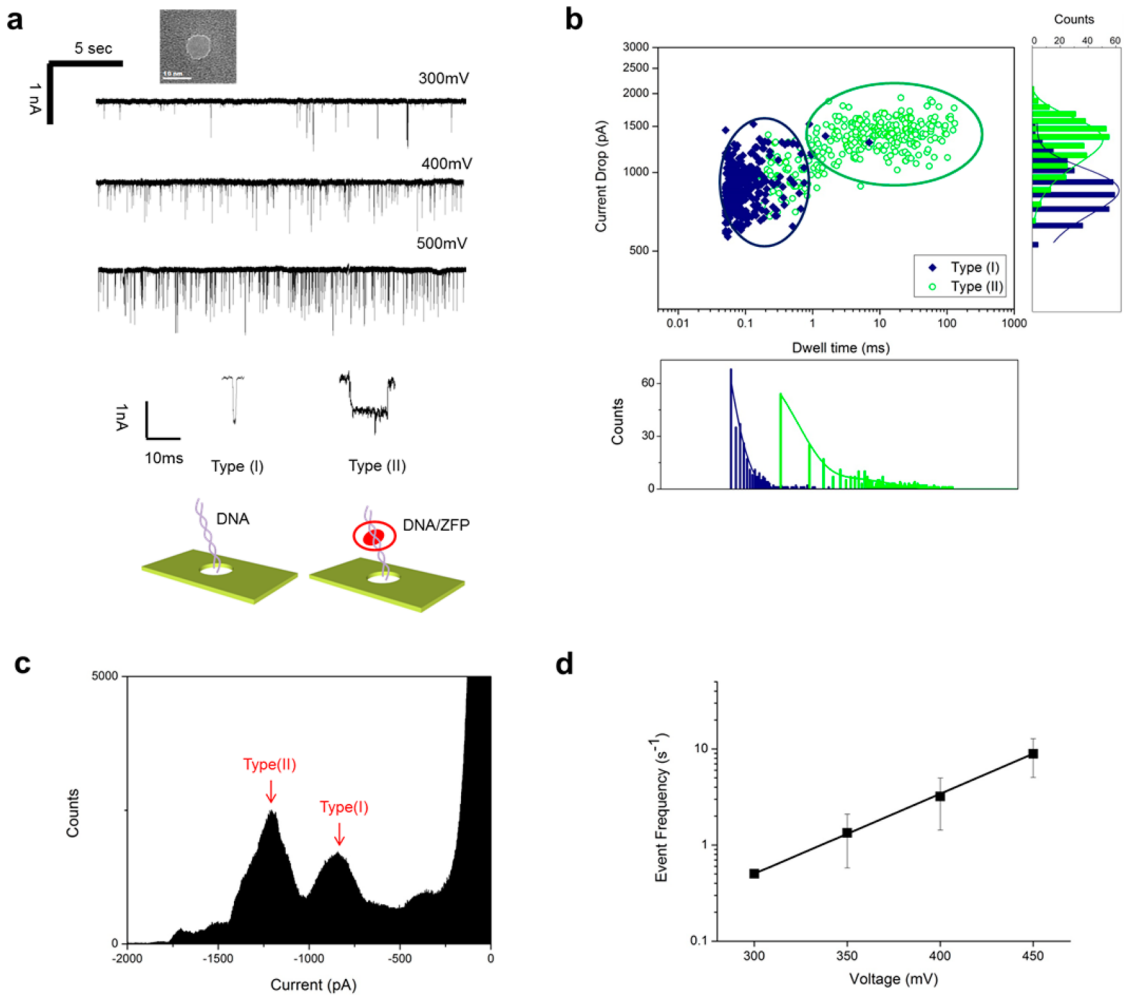

Figure 4. Analysis of DNA translocation events (5605 bp, binding site at 2-to-5 position) with ZFP in 500 mM KCl. (a) Current traces from the translocation of DNA-ZFP complex under three different applied voltages. Representative translocation signals from bare DNA (Type I) and DNA/ZFP (Type II) are shown. (b) Scatter plot of DNA translocation events (5605 bp)/ZFP through 7 nm nanopore on 20 nm thick SiN. Type (I) events were indicated as navy diamonds, and type (II) events were indicated as green circles, respectively. (c) All-point current histogram for DNA/ZFP translocations, showing discrete peaks for Type (I) and Type (II) events. (d) The frequency of translocation event as a function of applied voltage, which shows exponential increase of frequency upon increased voltage level.

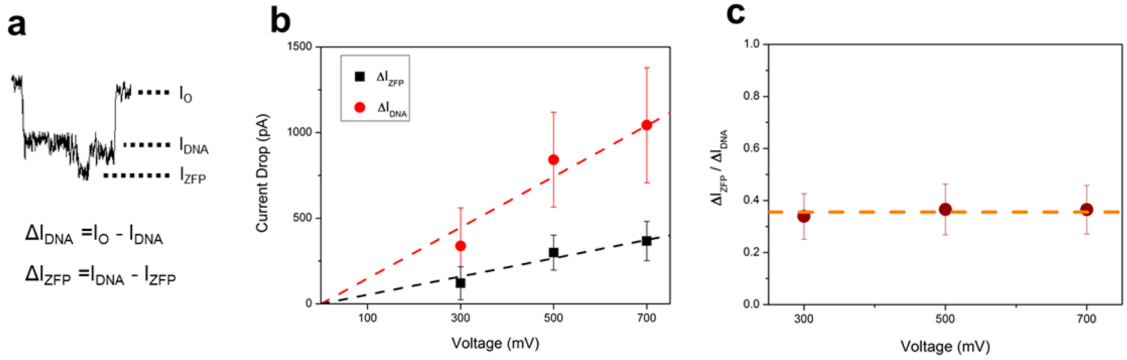

Figure 5. (a) A representative event signal of DNA (5606 bp)/ZFP translocations. Open pore current is indicated as I_O, the first current blockade level is I_{DNA}, and the additional current drop is I_{ZFP}. The first current drop magnitude from the open pore current ($I_O - I_{DNA}$) is indicated as ΔI_{DNA}, and the magnitude of the additional current drop ($I_{DNA} - I_{ZFP}$) is indicated as ΔI_{ZFP}. (b) Voltage dependency of ΔI_{DNA} and ΔI_{ZFP}. Both linearly increase with applied bias voltages. (c) Voltage dependency of $\Delta I_{ZFP}/\Delta I_{DNA}$. $\Delta I_{ZFP}/\Delta I_{DNA}$ is almost constant (~0.355) for three applied voltages.

indicate that the translocation velocity of the front part of the DNA that enters the nanopore first could be slightly lower than the latter part. Thus, the local DNA translocation velocity increases toward the end of

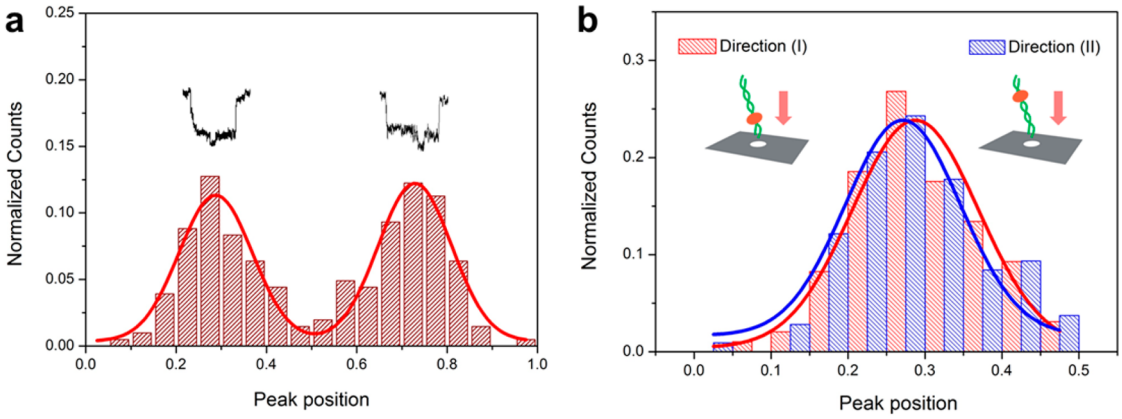

Figure 6. (a) Histogram of $t_1/(t_1 + t_2)$, where t_1 is assigned as the dwell time from the start of event to the additional spike and t_2 is assigned as the dwell time from the additional spike to the end of the event. Two Gaussian distributions were observed due to two opposite translocation directions. (b) Histogram of $t_1/(t_1 + t_2)$, where the shorter end of DNA from the ZFP binding site is analyzed as t_1 and the longer end is analyzed as t_2.

the translocation process, which is consistent with previous reports.[46,47]

Surprisingly, as demonstrated in the scatter plot of Figure 4b, type (II) events have a much longer translocation time than type (I) events. The delayed translocation of DNA with bound protein was also reported elsewhere with a somewhat different degree of delay.[29,31,48] The translocation time may have been delayed possibly due to protein adsorption to the pore walls or increased interactions of the bulky, less-charged DNA−protein complex with the pore. We presume that the following factors influence the slower DNA/ZFP complex translocation through the solid state nanopore: (i) The DNA/ZFP complex has a bulkier structure, and thus has stronger interactions with the pore walls than the bare DNA.[29,31,48] (ii) ZFP binding causes local uncoiling of dsDNA in the vicinity of the ZFP binding site. Relatively hydrophobic bases, both purines and pyrimidines, are normally buried within the double helical DNA structure but the uncoiling induced by ZFP binding could result in base exposure outward and may contribute to a greater interaction with the nanopore. A single stranded DNA with fully exposed bases has a greater interaction with the nanopore, which results in longer translocation time compared with a dsDNA.[49] (iii) Binding with positively charged ZFP in the tested environment would reduce the local negative charge of DNA because the electrophoretic force on DNA is proportional to the effective charge density of DNA.[50,51] (iv) Binding with ZFP increases the overall mass of DNA and thus increases dragging force during translocation. Although there is no clear-cut explanation for this slowing down effect, we speculate that all of these factors together may contribute to the delayed translocation of the DNA/ZFP complex. This result by itself may also suggest one way of controlling DNA translocation through the solid-state nanopore.

CONCLUSIONS

We have demonstrated the identifying of a protein binding site within a DNA to a single protein resolution using low noise solid-state nanopore. Characteristic ionic current signals arising from the passage of bare DNA and DNA/ZFP complexes enabled us to identify the location of the ZFP binding site within a DNA strand. ZFP is one of the most common transcriptional activators; thus, identification of the recognition locus within a long genomic DNA is important to understand biological phenomena and to design new drug or diagnostic tools. For this reason, nanopore technology is an ideal method to map the various ZFP binding sites along a long strand of DNA. Furthermore, our low noise nanopore device enabled us to detect the DNA/ZFP complex in a relatively low-salt environment. Because protein−DNA interactions are sensitive to salt concentrations, a reaction condition that is near physiological conditions may expand the application of nanopore devices for mapping or reading much useful genetic information in the near future.

MATERIALS AND METHODS

Nanopore Experiments. Low-stress LPCVD SiN_x 100 nm was deposited on 500 μm thick Si substrate. After photolithography and reactive ion etching, KOH wet etch was used to form freestanding SiN_x membrane (2 × 2 mm^2 window) on a 10 × 10 mm^2 Si chip. The SiN_x membrane was transferred onto Pyrex substrate, which is fabricated as previously described,[41] then the membrane was etched by CF_4 plasma to a desirable thickness (etch rate of ~15 nm/min). The nanopore was drilled into the transferred membrane by a highly focused electron beam using TEM. Prior to use, the nanopore was treated with oxygen plasma (15 mA, 30 s), and the nanopore chip was assembled in a custom-designed acrylic flow cell. After that, 500 mM KCl electrolyte solutions (buffered at pH 8.0 with

100 mM Tris-HCl) were introduced to the flow cell to hydrate the nanopore. The assembled nanopore cell was put in a dark Faraday cage, and then Ag/AgCl electrodes were connected to a patch clamp system and put into each chamber of the flow cell (cis and trans). In all of the experiments, the DNA concentration was set to 10 nM and the ZFP concentration was set to 4 times higher than the DNA. The ionic current was measured using the Axopatch 200B; the sampling rate was 250 kHz and was low-pass filtered with a 10 kHz Bessel filter. Translocation events were collected with Clampex 10.4 and further analyzed using Clampfit 10.4 software. To discriminate real translocations from bouncing spikes, we analyzed translocation events based on two common criteria, dwell time and current drop. Events having dwell time longer than 50 μs and current drop larger than 10 times of noise rms values are considered as real translocations.

Chemicals. Agar powder and sodium chloride (NaCl) were provided from Daejung Chemicals & Metals Co., Ltd. (Gyonggi-do, Korea). Luria−Bertani (LB) broth was purchased from BD (Difco, Lawrence, KS, USA). Ampicillin, isopropyl-β-D-thiogalactopyranoside (IPTG) and DL-dithiothreitol (DTT) were purchased from Biosesang (Gyonggi-do, Korea). The other chemicals such as T4 DNA ligase, *Not*I, *Pst*I and amylose resin were purchased from NEB (Ipswich, MA, USA), and Ethylenediaminetetraacetic acid (EDTA) was purchased from Biobasic (Markham, ON, Canada). Maltose monohydrate, zinc sulfate ($ZnSO_4$), magnesium chloride ($MgCl_2$), ethidium bromide and Coomassie blue were purchased from Sigma-Aldrich (St. Louis, MO, USA). The DNA ladder (100 bp), protein ladder (10 kDa) and Tris-HCl were from Noble bio (Gyonggi-do, Korea).

Expression and Purification of ZFP. Plasmids containing the Zif268//NRE zinc finger protein, pMal-c2x::*zfp* was kindly provided from Dr. Daniel Branton from the Department of Molecular and Cellular Biology at Harvard University. *E. coli* BL21 (DE3) harboring pMal-c2x::*zfp* plasmids were grown in 100 mL LB containing ampicillin (100 μg/mL) to an OD_{600} of 0.7−0.8 in a 37 °C shaking incubator (200 rpm) followed by the addition of 0.1 mM IPTG and grown overnight at 18 °C. Cells were then harvested by centrifugation at 4 °C for 20 min and resuspended in 5 mL column buffer (20 mM Tris-HCl, 200 mM NaCl, 1 mM EDTA, pH 7.4). The collected cells were disrupted by sonication for 10 min in an ice bath at 225 W (duty cycle 50%, VC 750, Sonics & Materials Inc., Newtown, CT, USA). After centrifugation at 4000 rpm for 20 min, the supernatant was retained and loaded onto a column packed with 600 μL amylose resin. The amylose column was washed with column buffer, and the zinc finger proteins were eluted by a column buffer containing 10 mM maltose. The purified zinc finger proteins were then identified and quantified by 8% SDS-PAGE and Bradford assay, respectively.

Preparation of dsDNA Strands Containing ZFP Binding Sites. Two types of dsDNAs with different lengths and ZFP binding positions were prepared to examine the possibility of detecting the location of recognition sequence using solid-state nanopore. Double-stranded DNA (5605 bp) with ZFP binding sites at the 2-to-5 position was constructed by inserting chemically synthesized oligonucleotides (5′-GGC CAA GGG TTC AGT GCG TGG GCG-3′ and 5′-GGC CCG CCC ACG CAC TGA ACC CTT-3′) with 20 bp of target sequence and NotI sites at both ends into the NotI site of pET21a(+) vectors. The plasmid containing ZFP binding sites was then linearized by enzymatic digestion with *Pst*I. Short dsDNA (520 bp) with ZFP binding site at the 1-to-1 position was prepared by PCR using a primer set (5′-AAA ACC CCT CAA GAC CCG TTT AGA-3′ and 5′-TGC CGG CCA CGA TGC GTC CGG CGT-3′) and purified pET21a(+) vectors containing ZFP binding sites as a template. For the gel shift assay, a pET21a(+) vector containing ZFP binding sites as a template and the primer set (5′-TCT AGA ACT AGT GGA TC-3′ and 5′-ATT AAC CCT CAC TAA AG-3′) were used to amplify 126 bp dsDNA with a ZFP binding sequence as a positive control. Double stranded DNA (134 bp) was used as a negative control without a ZFP binding sequence. It was prepared by amplification of the *Klebsiella pneumoniae* KCTC 2242 fimI gene using the primer set (5′-ATG CAG GGA ATG AAA TCT GGT CTG-3′ and 5′-CAT TAT CTC CTT GTC TGC TCA CCG-3′). The amplified DNA fragments were purified using a gel extraction kit prior to experiments.

Gel Shift Assay. Zinc finger protein and tested DNAs were incubated in 10 μL of 200 mM Tris-HCl (pH 7.0) containing 100 mM NaCl, 200 μM $ZnSO_4$, 10 mM $MgCl_2$ and 5 mM DTT at room temperature for 1 h.[4] Then, the reactions were run on 10% native polyacrylamide gel and stained with EtBr to visualize the location of DNA.[52]

AFM Analysis of the DNA-ZFP Complex. To visualize and confirm the location of ZFP on the DNA strand, the 520 bp DNA containing the ZFP binding site and the DNA-ZFP complex were imaged by AFM. After incubation of ZFP and DNA with a recognition site in a binding solution for 1 h at room temperature, $NiCl_2$ was added to the binding solutions at a final concentration of 10 mM to promote the adsorption of DNA molecules on the mica surface. 100 nM DNA and 40 nM ZFP were used as a final concentration in this analysis. Pristine DNA without ZFP was also examined to compare the DNA-ZFP complex morphology. A 20 μL sample solution was deposited on the freshly cleaved mica disc (10 mm in diameter), and the mica disc was washed with 3 mL of filtered distilled water after 10 min incubation at room temperature. The disc was then dried with a mild stream of nitrogen gas and stored in a vacuum desiccator until it was examined using AFM (XE-70, Park Systems, Suwon, Korea). Pristine DNA and the DNA-ZFP complex were then imaged in tapping mode with noncontact cantilever probes (PPP-NCHR, Park Systems) at a 0.3 Hz scan rate.

Conflict of Interest: The authors declare no competing financial interest.

Acknowledgment. We thank D. Branton for suggesting the use of nanopores to localize ZFP proteins on DNA strands. This research was supported by the National Research Foundation of Korea (NRF) grant that was funded by the Korean government (MEST) (2010-0017697) and the Pioneer Research Center Program (2012-0009563) through the National Research Foundation (NRF) of Korea that was funded by the Ministry of Science, ICT & Future Planning. This work was also supported by the Global Ph.D. Fellowship Program (2014H1A2A1016401) through the National Research Foundation of Korea (NRF), which was funded by the Ministry of Education.

Supporting Information Available: Figures regarding nanopore fabrication, device noise characteristics, and the effect of KCl concentration on ZFP-DNA dissociation. The Supporting Information is available free of charge on the ACS Publications website at DOI: 10.1021/acsnano.5b00784.

REFERENCES AND NOTES

1. Tupler, R.; Perini, G.; Green, M. R. Expressing the Human Genome. *Nature* **2001**, *409*, 832–833.
2. Klug, A. Co-Chairman'S Remarks: Protein Designs for the Specific Recognition of DNA. *Gene* **1993**, *135*, 83–92.
3. Posewitz, M. C.; Wilcox, D. E. Properties of the Sp1 Zinc Finger 3 Peptide: Coordination Chemistry, Redox Reactions, and Metal Binding Competition with Metallothionein. *Chem. Res. Toxicol.* **1995**, *8*, 1020–1028.
4. Kim, J.-S.; Pabo, C. O. Getting a Handhold on DNA: Design of Poly-Zinc Finger Proteins with Femtomolar Dissociation Constants. *Proc. Natl. Acad. Sci. U. S. A.* **1998**, *95*, 2812–2817.
5. Urnov, F. D.; Miller, J. C.; Lee, Y.-L.; Beausejour, C. M.; Rock, J. M.; Augustus, S.; Jamieson, A. C.; Porteus, M. H.; Gregory, P. D.; Holmes, M. C. Highly Efficient Endogenous Human Gene Correction using Designed Zinc-Finger Nucleases. *Nature* **2005**, *435*, 646–651.
6. Papworth, M.; Kolasinska, P.; Minczuk, M. Designer Zinc-Finger Proteins and Their Applications. *Gene* **2006**, *366*, 27–38.
7. Nakata, E.; Liew, F. F.; Uwatoko, C.; Kiyonaka, S.; Mori, Y.; Katsuda, Y.; Endo, M.; Sugiyama, H.; Morii, T. Zinc-Finger Proteins for Site-Specific Protein Positioning on DNA-Origami Structures. *Angew. Chem.* **2012**, *124*, 2471–2474.
8. Siggers, T.; Reddy, J.; Barron, B.; Bulyk, M. L. Diversification of Transcription Factor Paralogs *via* Noncanonical

Modularity in C2H2 Zinc Finger DNA Binding. *Mol. Cell* **2014**, *55*, 640–648.
9. Xu, S.; Wang, X.; Chen, J. Zinc Finger Protein 1 (ThZF1) from Salt Cress (*Thellungiella halophila*) is a Cys-2/His-2-type Transcription Factor Involved in Drought and Salt Stress. *Plant Cell Rep.* **2007**, *26*, 497–506.
10. Zimmerman, K. A.; Fischer, K. P.; Joyce, M. A.; Tyrrell, D. L. J. Zinc Finger Proteins Designed To Specifically Target Duck Hepatitis B Virus Covalently Closed Circular DNA Inhibit Viral Transcription in Tissue Culture. *J. Virol.* **2008**, *82*, 8013–8021.
11. Kim, S.; Gottfried, A.; Lin, R. R.; Dertinger, T.; Kim, A. S.; Chung, S.; Colyer, R. A.; Weinhold, E.; Weiss, S.; Ebenstein, Y. Enzymatically Incorporated Genomic Tags for Optical Mapping of DNA-Binding Proteins. *Angew. Chem., Int. Ed.* **2012**, *51*, 3578–3581.
12. Forget, A. L.; Dombrowski, C. C.; Amitani, I.; Kowalczykowski, S. C. Exploring Protein-DNA Interactions in 3D using *in situ* Construction, Manipulation and Visualization of Individual DNA Dumbbells with Optical Traps, Microfluidics and Fluorescence Microscopy. *Nat. Protoc.* **2013**, *8*, 525–538.
13. Chen, L.; Haushalter, K. A.; Lieber, C. M.; Verdine, G. L. Direct Visualization of a DNA Glycosylase Searching for Damage. *Chem. Biol.* **2002**, *9*, 345–350.
14. Wang, H.; Tessmer, I.; Croteau, D. L.; Erie, D. A.; Van Houten, B. Functional Characterization and Atomic Force Microscopy of a DNA Repair Protein Conjugated to a Quantum Dot. *Nano Lett.* **2008**, *8*, 1631–1637.
15. Nakata, E.; Liew, F. F.; Uwatoko, C.; Kiyonaka, S.; Mori, Y.; Katsuda, Y.; Endo, M.; Sugiyama, H.; Morii, T. Zinc-Finger Proteins for Site-Specific Protein Positioning on DNA-Origami Structures. *Angew. Chem., Int. Ed.* **2012**, *51*, 2421–2424.
16. Kim, M. J.; Wanunu, M.; Bell, D. C.; Meller, A. Rapid Fabrication of Uniformly Sized Nanopores and Nanopore Arrays for Parallel DNA Analysis. *Adv. Mater.* **2006**, *18*, 3149–3153.
17. Dekker, C. Solid-State Nanopores. *Nat. Nanotechnol.* **2007**, *2*, 209–215.
18. Branton, D.; Deamer, D. W.; Marziali, A.; Bayley, H.; Benner, S. A.; Butler, T.; Di Ventra, M.; Garaj, S.; Hibbs, A.; Huang, X.; *et al.* The Potential and Challenges of Nanopore Sequencing. *Nat. Biotechnol.* **2008**, *26*, 1146–1153.
19. Oukhaled, A.; Cressiot, B.; Bacri, L.; Pastoriza-Gallego, M.; Betton, J.-M.; Bourhis, E.; Jede, R.; Gierak, J.; Auvray, L.; Pelta, J. Dynamics of Completely Unfolded and Native Proteins through Solid-State Nanopores as a Function of Electric Driving Force. *ACS Nano* **2011**, *5*, 3628–3638.
20. Niedzwiecki, D. J.; Grazul, J.; Movileanu, L. Single-Molecule Observation of Protein Adsorption onto an Inorganic Surface. *J. Am. Chem. Soc.* **2010**, *132*, 10816–10822.
21. Li, J.; Gershow, M.; Stein, D.; Brandin, E.; Golovchenko, J. A. DNA Molecules and Configurations in a Solid-State Nanopore Microscope. *Nat. Mater.* **2003**, *2*, 611–615.
22. Fologea, D.; Uplinger, J.; Thomas, B.; McNabb, D. S.; Li, J. Slowing DNA Translocation in a Solid-State Nanopore. *Nano Lett.* **2005**, *5*, 1734–1737.
23. Smeets, R. M. M.; Keyser, U. F.; Krapf, D.; Wu, M.-Y.; Dekker, N. H.; Dekker, C. Salt Dependence of Ion Transport and DNA Translocation through Solid-State Nanopores. *Nano Lett.* **2005**, *6*, 89–95.
24. Fologea, D.; Ledden, B.; McNabb, D. S.; Li, J. Electrical Characterization of Protein Molecules by a Solid-State Nanopore. *Appl. Phys. Lett.* **2007**, 91.
25. Talaga, D. S.; Li, J. Single-Molecule Protein Unfolding in Solid State Nanopores. *J. Am. Chem. Soc.* **2009**, *131*, 9287–9297.
26. Wanunu, M.; Dadosh, T.; Ray, V.; Jin, J.; McReynolds, L.; Drndic, M. Rapid Electronic Detection of Probe-Specific MicroRNAs Using Thin Nanopore Sensors. *Nat. Nanotechnol.* **2010**, *5*, 807–814.
27. Japrung, D.; Dogan, J.; Freedman, K. J.; Nadzeyka, A.; Bauerdick, S.; Albrecht, T.; Kim, M. J.; Jemth, P.; Edel, J. B. Single-Molecule Studies of Intrinsically Disordered Proteins Using Solid-State Nanopores. *Anal. Chem.* **2013**, *85*, 2449–2456.
28. Kowalczyk, S. W.; Hall, A. R.; Dekker, C. Detection of Local Protein Structures along DNA Using Solid-State Nanopores. *Nano Lett.* **2009**, *10*, 324–328.
29. Singer, A.; Wanunu, M.; Morrison, W.; Kuhn, H.; Frank-Kamenetskii, M.; Meller, A. Nanopore Based Sequence Specific Detection of Duplex DNA for Genomic Profiling. *Nano Lett.* **2010**, *10*, 738–742.
30. Singer, A.; Rapireddy, S.; Ly, D. H.; Meller, A. Electronic Barcoding of a Viral Gene at the Single-Molecule Level. *Nano Lett.* **2012**, *12*, 1722–1728.
31. Japrung, D.; Bahrami, A.; Nadzeyka, A.; Peto, L.; Bauerdick, S.; Edel, J. B.; Albrecht, T. SSB Binding to Single-Stranded DNA Probed Using Solid-State Nanopore Sensors. *J. Phys. Chem. B* **2014**, *118*, 11605–11612.
32. Carlsen, A. T.; Zahid, O. K.; Ruzicka, J. A.; Taylor, E. W.; Hall, A. R. Selective Detection and Quantification of Modified DNA with Solid-State Nanopores. *Nano Lett.* **2014**, *14*, 5488–5492.
33. Bell, N. A. W.; Keyser, U. F. Specific Protein Detection Using Designed DNA Carriers and Nanopores. *J. Am. Chem. Soc.* **2015**, *137*, 2035–2041.
34. Mahmood, M. A. I.; Ali, W.; Adnan, A.; Iqbal, S. M. 3D Structural Integrity and Interactions of Single-Stranded Protein-Binding DNA in a Functionalized Nanopore. *J. Phys. Chem. B* **2014**, *118*, 5799–5806.
35. Wang, H.; Hurt, N.; Dunbar, W. B. Measuring and Modeling the Kinetics of Individual DNA–DNA Polymerase Complexes on a Nanopore. *ACS Nano* **2013**, *7*, 3876–3886.
36. Van Meervelt, V.; Soskine, M.; Maglia, G. Detection of Two Isomeric Binding Configurations in a Protein–Aptamer Complex with a Biological Nanopore. *ACS Nano* **2014**, *8*, 12826–12835.
37. Wang, H.-Y.; Li, Y.; Qin, L.-X.; Heyman, A.; Shoseyov, O.; Willner, I.; Long, Y.-T.; Tian, H. Single-Molecule DNA Detection Using a Novel SP1 Protein Nanopore. *Chem. Commun.* **2013**, *49*, 1741–1743.
38. Pomerantz, J. L.; Wolfe, S. A.; Pabo, C. O. Structure-Based Design of a Dimeric Zinc Finger Protein. *Biochemistry* **1998**, *37*, 965–970.
39. Moore, M.; Choo, Y.; Klug, A. Design of Polyzinc Finger Peptides with Structured Linkers. *Proc. Natl. Acad. Sci. U. S. A.* **2001**, *98*, 1432–1436.
40. Storm, A. J.; Chen, J. H.; Ling, X. S.; Zandbergen, H. W.; Dekker, C. Fabrication of Solid-State Nanopores with Single-Nanometre Precision. *Nat. Mater.* **2003**, *2*, 537–540.
41. Lee, M.-H.; Kumar, A.; Park, K.-B.; Cho, S.-Y.; Kim, H.-M.; Lim, M.-C.; Kim, Y.-R.; Kim, K.-B. A Low-Noise Solid-State Nanopore Platform Based on a Highly Insulating Substrate. *Sci. Rep.* **2014**, 4.
42. Brinkers, S.; Dietrich, H. R. C.; de Groote, F. H.; Young, I. T.; Rieger, B. The Persistence Length of Double Stranded DNA Determined using Dark Field Tethered Particle Motion. *J. Chem. Phys.* **2009**, 130.
43. Wanunu, M.; Sutin, J.; McNally, B.; Chow, A.; Meller, A. DNA Translocation Governed by Interactions with Solid-State Nanopores. *Biophys. J.* **2008**, *95*, 4716–4725.
44. Chen, P.; Gu, J.; Brandin, E.; Kim, Y.-R.; Wang, Q.; Branton, D. Probing Single DNA Molecule Transport Using Fabricated Nanopores. *Nano Lett.* **2004**, *4*, 2293–2298.
45. Storm, A. J.; Chen, J. H.; Zandbergen, H. W.; Dekker, C. Translocation of Double-Strand DNA through a Silicon Oxide Nanopore. *Phys. Rev. E: Stat., Nonlinear, Soft Matter Phys.* **2005**, *71*, 051903.
46. Lu, B.; Albertorio, F.; Hoogerheide, D. P.; Golovchenko, J. A. Origins and Consequences of Velocity Fluctuations during DNA Passage through a Nanopore. *Biophys. J.* **2011**, *101*, 70–79.
47. Plesa, C.; van Loo, N.; Ketterer, P.; Dietz, H.; Dekker, C. Velocity of DNA during Translocation through a Solid-State Nanopore. *Nano Lett.* **2014**, *15*, 732–737.
48. Shim, J.; Humphreys, G. I.; Venkatesan, B. M.; Munz, J. M.; Zou, X.; Sathe, C.; Schulten, K.; Kosari, F.; Nardulli, A. M.; Vasmatzis, G.; *et al.* Detection and Quantification of Methylation in DNA using Solid-State Nanopores. *Sci. Rep.* **2013**, 3.

49. Aksimentiev, A.; Heng, J. B.; Timp, G.; Schulten, K. Microscopic Kinetics of DNA Translocation through Synthetic Nanopores. *Biophys. J.* **2004**, *87*, 2086–2097.
50. Meller, A.; Nivon, L.; Branton, D. Voltage-Driven DNA Translocations through a Nanopore. *Phys. Rev. Lett.* **2001**, *86*, 3435–3438.
51. Keyser, U. F.; Koeleman, B. N.; van Dorp, S.; Krapf, D.; Smeets, R. M. M.; Lemay, S. G.; Dekker, N. H.; Dekker, C. Direct Force Measurements on DNA in a Solid-State Nanopore. *Nat. Phys.* **2006**, *2*, 473–477.
52. Mackay, J. P.; Segal, D. J. *Engineered Zinc Finger Proteins: Methods and Protocols*; Humana Press: New York, 2010.